Non-stationary Characteristics for Indoor Massive MIMO Channels

Qi Wang(✉), Jiadong Du, and Yuanyuan Cui

China Academy of Information and Communications Technology, Beijing 100191, China
qiwang.609@gmail.com

Abstract. Massive Multiple Input Multiple Output (MIMO) has been widely considered as one of the most promising technologies for the fifth-generation (5G) wireless communication. In massive MIMO system, the research on channel characteristics is important. In this paper, the characteristics for massive MIMO channels at both 2 GHz and 6 GHz are investigated. Based on the real-world measurements, the channel parameters in the delay and frequency domains are extracted to show the non-stationary phenomenon over the large-scale antenna array. Furthermore, the characteristics of the angular parameters extracted by space-alternating generalized expectation-maximization (SAGE) algorithm are investigated and the fluctuations are modeled. The results for different frequencies are useful for deep understanding of massive MIMO channels in the future.

Keywords: Massive MIMO · Channel characteristics · Angular parameter

1 Introduction

Nowadays, the fifth-generation (5G) wireless communication is a very hot topic in both academic and industry fields [1]. The key capabilities of 5G systems will dramatically outperform the previous generation systems. In general, 5G is expected to have more than 5 times improvement on spectrum efficiency and more than 100 times improvement on energy and cost efficiency [2]. To fulfill the requirements of 5G, massive Multiple Input Multiple Output (MIMO) technology has been introduced and regarded as one of the most important technologies in 5G system.

This work was supported by the Science and Technology Foundation of the State Grid Corporation of China: Adaptability research and application between LTE wireless private network and electric power service.

X. Liu et al. (Eds.): ChinaCom 2018, LNICST 262, pp. 384–393, 2019.
https://doi.org/10.1007/978-3-030-06161-6_38

Some key issues for massive MIMO have already been figured out in recent years. As the foundation of wireless communication, the deep understanding of propagation channel is of importance. However, the researches on channel characteristics and modeling approaches are still open issues for massive MIMO. In a massive MIMO system, a large number of antennas will be equipped at the base stations [3]. Therefore, the massive MIMO channel characteristics should be obviously different from the traditional MIMO channels. Channel measurements for massive MIMO have been performed in various of scenarios, such as outdoor campus [4,5], indoor scenario [6], and indoor venue [7]. Different antenna array shapes have been adopted for massive MIMO measurements, which include 128-element linear and cylindrical array [8,9], 112-element scalable virtual antenna array [10], and 64-element switch array with different shapes [6], respectively. Based on the measurement results, channel characteristics such as channel gain, delay spread, Ricean K-factor, and angular power spectrum are analyzed, and the non-stationary phenomenon over the large-scale antenna array has been discovered [8]. However, the differences between channel characteristics at different frequencies in massive MIMO channels are not considered in the existing measurements. Moreover, the channel behaviors in some typical 5G scenario are not fully addressed.

Hence, channel measurements at both 2 GHz and 6 GHz in an indoor hall scenario have been briefly introduced in this paper. The non-stationary phenomenon over the large-scale antenna array has been presented by the obtained statistical parameters in the delay and frequency domains, and these behaviors at different frequencies are further explained. Finally, the characteristics of the channel angular parameters are investigated, and the non-stationarity of these parameters is modeled.

The rest of this paper is organized as follows. The massive MIMO channel characteristics at different central frequencies are presented in Sect. 2. Section 3 describes the characteristics and modeling of angular parameters. Finally, Sect. 4 concludes the paper.

2 Massive MIMO Channel Characteristics

2.1 Measurement Description

The measurement environment was selected in an indoor hall scenario, which was expected to have ultra-high connections during the events. The transmitter (Tx) antenna was a 64-element virtual linear antenna array generated by using a high-accuracy automatic turntable, thus the Tx array could be regarded as a large-scale antenna array. At the receiver (Rx) side, a 4-element linear antenna array was constituted by moving one single antenna manually. The central frequency of the measurements was selected as 2 GHz or 6 GHz with a bandwidth of 200 MHz, so as to compare the channel characteristics at different propagation frequencies. Note that both 2 GHz and 6 GHz are considered as the alternative frequencies for the massive MIMO system in 5G. During the measurements, both the line-of-sight (LOS) and the non-LOS (NLOS) cases were considered, and the NLOS case

was realized by placing the Rx antenna array below the seats. Moreover, a multi-carrier signal in the frequency domain was utilized to measure the channels by the self-designed channel sounder system. Thus, the wideband channel transfer function (CTF) between the m-th Tx antenna and the n-th Rx antenna can be obtained from the recorded IQ data, which can be expressed as $H(m, n, \tau)$, and τ is the multipath delay. Finally, all the details of the measurement scenario and system can be found in [11].

2.2 Power Delay Profile

The channel impulse response (CIR) $h(m, n, \tau)$ can be obtained from the inverse Fourier transform of the CTF $H(m, n, \tau)$. The power delay profile (PDP) and the corresponding average PDP (APDP) along the Tx antenna array APDP (m, τ) can then be calculated according to the method in [11]. It is noted that the effective multipath components (MPCs) are extracted by using the power threshold selected as the noise floor of measurement system plus 6 dB [12].

The root mean square (RMS) delay spreads (DSs) can therefore be computed based on APDPs

$$\sigma_\tau = \sqrt{\frac{\int_0^\infty \tau^2 \mathrm{APDP}(m,\tau)d\tau}{\int_0^\infty \mathrm{APDP}(m,\tau)d\tau} - \overline{\tau}^2}, \tag{1}$$

where $\overline{\tau}$ is the mean delay, and can be expressed as

$$\overline{\tau} = \frac{\int_0^\infty \tau \mathrm{APDP}(m,\tau)d\tau}{\int_0^\infty \mathrm{APDP}(m,\tau)d\tau}. \tag{2}$$

The RMSDSs for different conditions are illustrated in Fig. 1. It is noticed that the RMSDSs in the LOS condition are roughly smaller than the values in the NLOS condition across the large-scale array at both 2 GHz and 6 GHz. However, the RMSDSs in the NLOS case are just slightly larger than the values in the LOS case at 2 GHz, which can be explained by a combination of smaller free space path loss and penetration loss at the lower frequency, i.e., the NLOS condition in such an indoor hall scenario is more like an obstructed LOS condition at 2 GHz. One can observe that the received power difference between LOS and NLOS cases is larger in the 6 GHz case than in the 2 GHz case. Diffraction over the seats will also be somewhat stronger at the lower frequency. Worth noting is the unexpected and fairly large variation of the LOS component in the 2 GHz LOS case. At present we do not have a good explanation for this phenomenon. One hypothesis is a stronger two-ray condition from the floor reflection at 2 GHz, yielding lower received power around the center of the array. Finally, the statistics of RMSDS are summarized in Table 1.

2.3 Frequency Correlation Function

The frequency correlation function (FCF) of the m-th Tx position, which can be obtained from the Fourier transform of the APDP of the m-th Tx position, is defined as [13]

$$R_H(m, \Delta f) = \int_{-\infty}^{+\infty} \mathrm{APDP}(m, \tau) \cdot e^{-j2\pi \Delta f \tau} d\tau, \tag{3}$$

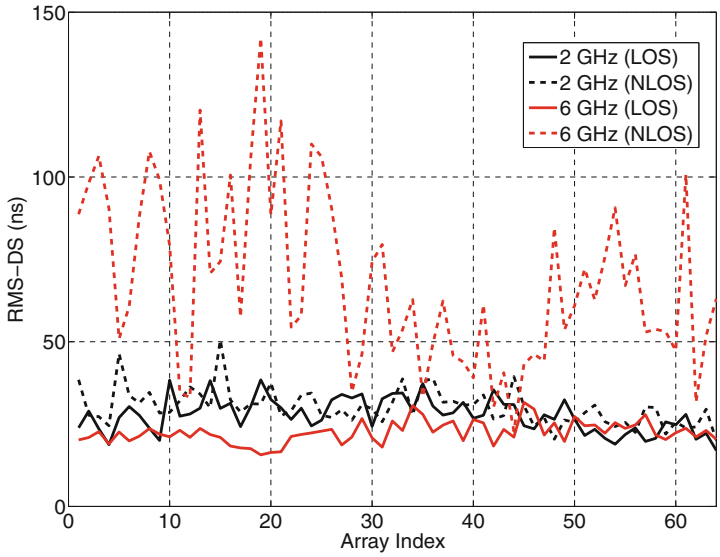

Fig. 1. RMSDSs under different conditions at 2 GHz and 6 GHz.

Table 1. Statistics of RMSDSs in nanoseconds under different conditions at 2 GHz and 6 GHz

Condition	Minimum value	Maximum value	Mean value	Standard deviation (Std)
2 GHz (LOS)	16.99	38.42	27.71	5.17
2 GHz (NLOS)	20.05	50.51	30.15	5.59
6 GHz (LOS)	15.64	31.56	22.48	3.32
6 GHz (NLOS)	22.82	142.2	68.13	26.31

where the Δf is the frequency difference. The measured FCFs at 2 GHz and 6 GHz across the Tx array are therefore obtained. The coherence bandwidth B_{coh} can then be defined as a bandwidth at which the correlation drops to a value of

$1/e$. Here also we might draw the same conclusion that non-stationarity exists for both 2 GHz and 6 GHz with different extents. Figure 2 gives the coherence bandwidth across the Tx array. As expected, the NLOS values of coherence bandwidth are generally smaller than those for the LOS case at 6 GHz, but there is no clear dependency at 2 GHz. Also, it can be observed that the values vary significantly over the large-scale antenna array at both center frequencies. Finally, the statistics of coherence bandwidths are summarized in Table 2.

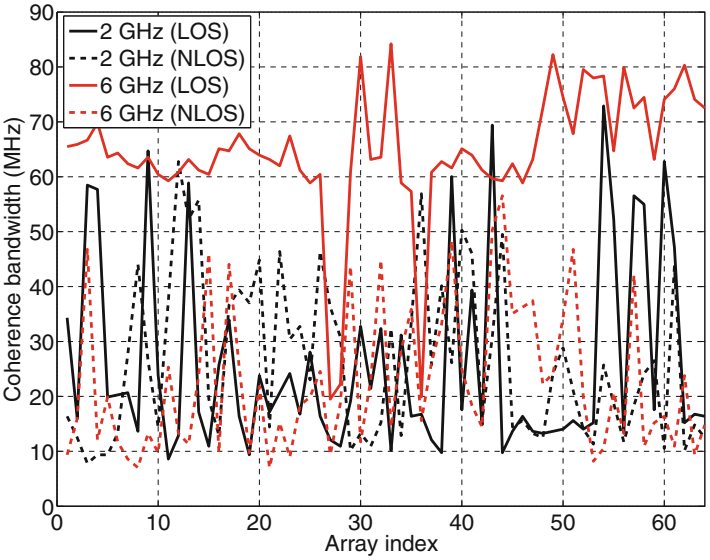

Fig. 2. Coherence bandwidths under different conditions at 2 GHz and 6 GHz.

Table 2. Statistics of coherence bandwidths in MHz under different conditions at 2 GHz and 6 GHz

Condition	Minimum value	Maximum value	Mean value	Standard deviation (Std)
2 GHz (LOS)	8.58	72.90	25.96	17.80
2 GHz (NLOS)	7.80	62.77	26.27	14.51
6 GHz (LOS)	19.49	84.21	64.42	12.00
6 GHz (NLOS)	7.02	56.53	22.64	13.16

3 Non-stationary Characteristics of Angular Parameters

In this section, the non-stationarity on the angular characteristics over the large-scale antenna array at different frequencies is further investigated, and the fluctuations of different statistical parameters in the angular domain are also modeled. Note that the characteristics in the delay domain can be found in [14].

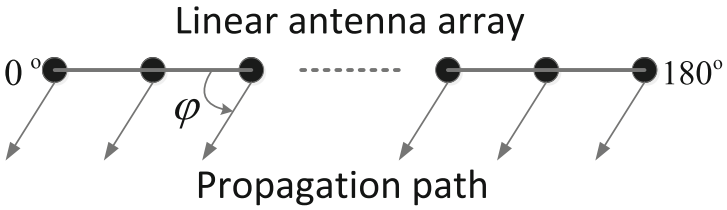

Fig. 3. Definition of the propagation path at the Tx side.

To obtain the angular parameters of MPCs, the space-alternating generalized expectation-maximization (SAGE) algorithm is adopted. The number of MPCs in SAGE is chosen as 80, and the delay resolution is 5 ns, which is the same with the measurement system. As the linear antenna array at the TX side is used in our measurements, the azimuth angle of departure (AOD) over the large-scale antenna array can be estimated in SAGE, which ranges from 0° to 180° as defined in Fig. 3. Therefore, the MPCs with the same propagation delay can be further distinguished as different MPCs based on the estimated AODs, and the CIR of each MPC can be expressed as $h\,(n, m, \tau, \varphi)$, compared to the CIR of MPC $h\,(n, m, \tau)$ without the angular information. The φ is the azimuth AOD estimated for each MPC in the SAGE algorithm. The power azimuth spectrum (PAS) of each sub-channel between the m-th Tx antenna and the n-th Rx antenna can therefore be computed as

$$P(\varphi) = \sum_{l=1}^{L} \delta(\varphi - \varphi_l) |h\,(n, m, \tau, \varphi)|^2, \tag{4}$$

where L is the number of MPCs, which equals to 80. By using the $P(\varphi)$, the statistical parameters in the angular domain can be obtained.

The root mean square azimuth spread (RMSAS) at each Tx position is defined by

$$\sigma_\varphi = \sqrt{\frac{\sum\limits_{\varphi=0^\circ}^{180^\circ} |\varphi - \mu_\varphi|^2 P(\varphi)}{\sum\limits_{\varphi=0^\circ}^{180^\circ} P(\varphi)}}, \tag{5}$$

where μ_φ is the mean angular value of the PAS at each TX position, and can be calculated as

$$\mu_\varphi = \frac{\sum\limits_{\varphi=0^\circ}^{180^\circ} \varphi P(\varphi)}{\sum\limits_{\varphi=0^\circ}^{180^\circ} P(\varphi)}. \tag{6}$$

Similar to RMSDS, the spatial dispersion in the angular domain can be described by RMSAS. Finally, the maximum value of the PAS is defined by

$$\varphi^{\max} = \underset{\varphi\in[0°,180°]}{\arg\max}\,(P(\varphi)), \tag{7}$$

which gives the AOD of the dominant MPC under any conditions.

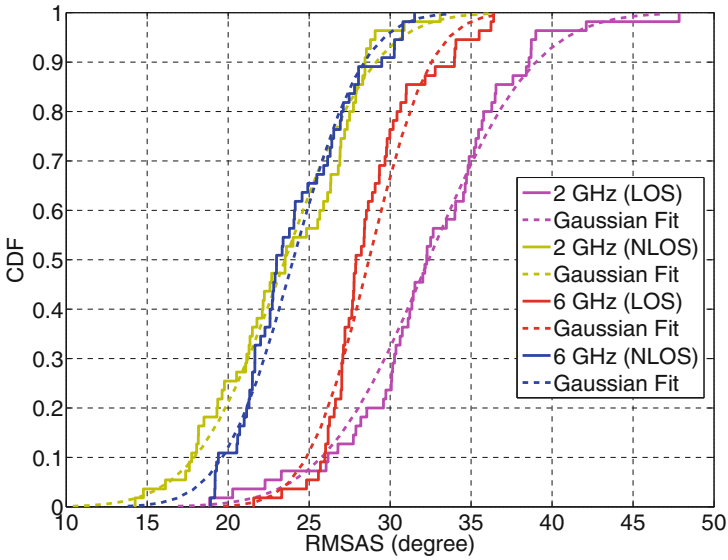

Fig. 4. CDFs of the RMSAS under different conditions at 2 GHz and 6 GHz.

The fluctuations of RMSASs across the large-scale antenna array at different frequencies are aimed to be modeled, so as to characterize the differences of non-stationarity between different frequencies. However, no clear trends can be discovered for the angular parameters over the large-scale antenna array. Thus, it can be concluded that the statistical angular parameters change irregularly for different antenna positions, and the cumulative distribution functions (CDFs) of the RMSASs under different conditions at both 2 GHz and 6 GHz are plotted in Fig. 4. It can be observed that the range of RMSASs at 2 GHz in the LOS condition is larger than the ranges in other three cases, which agrees with the result in Sect. 2.3 where this case was found to have the largest degree of non-stationarity. We can also see that RMSASs in the LOS conditions are larger than the values in the NLOS conditions at both 2 GHz and 6 GHz. This can be explained that the NLOS condition in our measurement is more like the obstructed LOS condition due to the limited measurement spaces, and most of the MPCs with large AODs are blocked by the seats. According to the results

in [11], the dominant MPCs in the NLOS conditions are the ground reflection path and the diffracted path over the seats, and the AODs of these paths regarding to the AOD of LOS path are very small. With larger path loss and penetration loss, this phenomenon is more distinct at 6 GHz.

As also shown in Fig. 4, the CDFs of RMSASs under different conditions at both 2 GHz and 6 GHz can all be well modeled by the Gaussian distributions. By adopting the Kolmogorov–Smirnov (KS) testing, the goodness of all these fittings have been tested. The measured values and Gaussian fit values of RMSASs are further summarized in Table 3. From the results of modeled standard deviation, one can also draw a conclusion that the fluctuations of RMSASs are positively correlated to the non-stationarity characterized by collinearity [11] in different conditions.

Table 3. Statistics of RMSASs under different conditions at 2 GHz and 6 GHz

Condition	Measured values		Gaussian fit values	
	Median	90th percentile	Mean	Std
2 GHz (LOS)	32.26°	38.58°	31.89°	9.09°
2 GHz (NLOS)	23.52°	28.45°	23.41°	7.94°
6 GHz (LOS)	27.89°	33.97°	28.19°	5.34°
6 GHz (NLOS)	22.99°	29.48°	23.80°	6.21°

As the strongest path in each condition, the maximum value $\varphi^{\max}$ of the PAS over the large-scale antenna array is investigated. Obviously, the maximum value $\varphi^{\max}$ in the LOS condition can be expressed as

$$\varphi^{\max} = \varphi_{LOS}, \tag{8}$$

and φ_{LOS} is the AOD for the LOS path, which can be simply calculated by the geometry. However, $\varphi^{\max}$ in the NLOS condition is more difficult to determine. Figure 5 gives the maximum value $\varphi^{\max}$ of the PAS over the large-scale antenna array in the NLOS conditions. As discussed above, a potentially strong diffracted path (and possibly a floor reflected path) still exists in some sub-channels, and these paths have similar AOD to that of the LOS path in this position. Thus, based on the results in Fig. 5, the maximum value $\varphi^{\max}$ in the NLOS condition is modeled as

$$\varphi^{\max} = \varphi_{LOS} + \sigma_{\varphi}, \tag{9}$$

where σ_{φ} is the standard deviation of the $\varphi^{\max}$ at each center frequency. The values of σ_{φ} are calculated and listed in Table 4.

Table 4. Standard deviation of the value σ_φ in the NLOS condition

	2 GHz	6 GHz
σ_φ	5.84°	4.01°

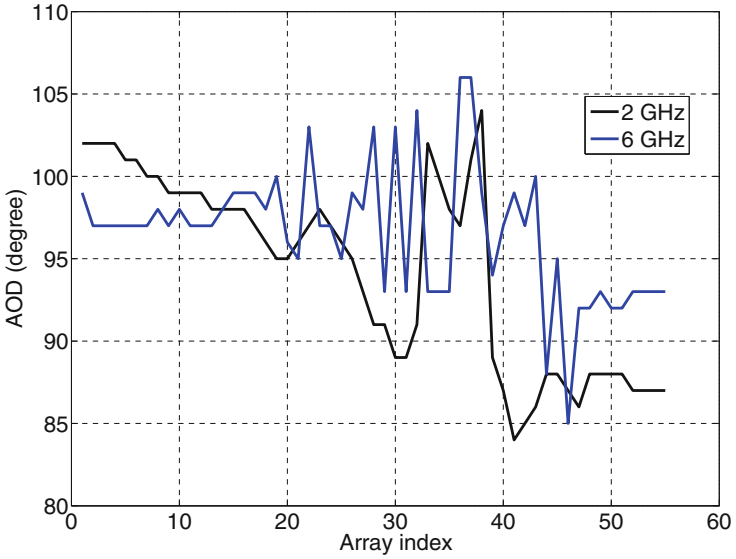

Fig. 5. Maximum value of the PAS over the large-scale antenna array in the NLOS condition.

4 Conclusion

The massive MIMO channel characteristics at both 2 GHz and 6 GHz have been presented in this paper. The non-stationary phenomenon across the large-scale antenna array were investigated by the obtained statistical parameters in the delay and frequency domains. It was found that the RMSDSs and the coherence bandwidths over the large-scale antenna array were clearly different in different conditions, and the statistical values were also provided in this paper. Furthermore, the RMSAS and the maximum value of the PAS over the large-scale antenna array were investigated, and the median values of RMSAS ranged from 22.99° to 32.26° under different cases. Finally, the non-stationarity models of these angular parameters were further established. These results should be useful for deep understanding of massive MIMO channels in the future.

References

1. Gohil, A., Modi, H., Patel, S.: 5G technology of mobile communication: a survey. In: 2013 International Conference on Intelligent Systems and Signal Processing (ISSP), pp. 288–292. IEEE, Gujarat, India (2013)

2. IMT-2020 Promotion Group: 5G vision and requirements. http://www.imt-2020.org.cn/en. Accessed May 2014
3. Jungnickel, V., et al.: The role of small cells, coordinated multipoint, and massive MIMO in 5G. IEEE Commun. Mag. **52**(5), 44–51 (2014)
4. Payami, S., Tufvesson, F.: Channel measurements and analysis for very large array systems at 2.6 GHz. In: 2012 6th European Conference on Antennas and Propagation (EUCAP), pp. 433–437. IEEE, Prague, Czech Republic (2012)
5. Payami, S., Tufvesson, F.: Delay spread properties in a measured massive MIMO system at 2.6 GHz. In: 2013 IEEE 24th Annual International Symposium on Personal, Indoor, and Mobile Radio Communications (PIMRC), pp. 53–57. IEEE, London, UK (2013)
6. Gauger, M., Hoydis, J., Hoek, C., Schlesinger, H., Pascht, A., Brink, S.: Channel measurements with different antenna array geometries for massive MIMO systems. In: 10th International ITG Conference on Systems, Communications and Coding (SCC), pp. 1–6. IEEE, Hamburg, Germany (2015)
7. Martinez, A., Carvalho, E., Nielsen, J.: Towards very large aperture massive MIMO: a measurement based study. In: 2014 IEEE Globecom Workshops (GC Wkshps), pp. 281–286. IEEE, Austin, USA (2014)
8. Gao, X., Edfors, O., Rusek, F., Tufvesson, F.: Massive MIMO performance evaluation based on measured propagation data. IEEE Trans. Wirel. Commun. **14**(7), 3899–3911 (2015)
9. Gao, X., Edfors, O., Tufvesson, F., Larsson, E.: Massive MIMO in real propagation environments: do all antennas contribute equally? IEEE Trans. Commun. **63**(11), 3917–3928 (2015)
10. Hoydis, J., Hoek, C., Wild, T., Brink, S.: Channel measurements for large antenna arrays. In: 2012 International Symposium on Wireless Communication Systems (ISWCS), pp. 811–815. IEEE, Paris, France (2012)
11. Wang, Q., et al.: Spatial variation analysis for measured indoor massive MIMO channels. IEEE Access **5**, 20828–20840 (2017)
12. Molisch, A., Steinbauer, M.: Condensed parameters for characterizing wideband mobile radio channels. Int. J. Wirel. Inf. Netw. **6**(3), 133–154 (1999)
13. Molisch, A.: Wireless Communications, 2nd edn. Wiley, Hoboken (2010)
14. Li, J., et al.: Measurement-based characterizations of indoor massive MIMO channels at 2 GHz, 4 GHz, and 6 GHz frequency bands. In: 2016 IEEE 83rd Vehicular Technology Conference (VTC Spring), pp. 1–5. IEEE, Nanjing, China (2016)